ISIJ International, Vol. 44 (2004), No. 11, pp. 1894–1901

Cold Swaging, Recovery and Recrystallization of Oligocrystalline INCOLOY MA 956—Part I: Deformed State

Marcio Ferreira HUPALO, Angelo Fernando PADILHA, Hugo Ricardo Zschommler SANDIM[1] and Andrea Madeira KLIAUGA[2]

Departamento de Engenharia Metalúrgica e de Materiais, Escola Politécnica, Universidade de São Paulo, Sao Paulo, SP, 05508-900, Brazil. E-mail: padilha@usp.br 1) Departamento de Engenharia de Materiais, Faculdade de Engenharia Química de Lorena, P.O.Box 116, Lorena, SP, 12600-970, Brazil. 2) Departamento de Engenharia de Materiais, Universidade Federal de São Carlos, Rodovia Washington Luís (SP-310), km 235, São Carlos, SP, 13565-905, Brazil.

(*Received on May 17, 2004; accepted in final form on August 10, 2004*)

Oxide dispersion strengthened (ODS) superalloys combine high temperature strength and excellent corrosion and oxidation resistances. INCOLOY MA 956 is an iron-based ODS superalloy containing about 1 % (volume) of fine and uniformly dispersed Y_2O_3 particles in a ferritic matrix. In the present work a coarse-grained (oligocrystalline) bar of MA 956 alloy was cold deformed by rotary swaging to reductions in area of 20, 47, 61, and 72 %. Microstructural characterization of deformed samples was performed using light optical microscopy (LOM), X-ray diffraction (XRD), electron backscatter diffraction (EBSD), and Vickers microhardness testing. The microstructure in the deformed state was found to be very inhomogeneous. Deformation bands were observed in all grains. The extent of deformation banding varies from grain to grain in terms of morphology and spacing. The deformation substructures were found to be very different in each grain. A sharp ⟨110⟩-fiber texture was developed during plastic deformation becoming more pronounced with increasing strain.

KEY WORDS: INCOLOY MA 956; mechanical alloying; cold swaging; work hardening; microstructure; texture; EBSD.

1. Introduction

INCOLOY®* MA 956 is an oxide dispersion strengthened (ODS) iron-based superalloy produced by mechanical alloying (MA) techniques. It has the following nominal chemical composition: Fe–20%Cr–4.5%Al–0.5%Ti–0.5%Y_2O_3 (in wt%).[1)] The alloy has excellent mechanical strength and resistance to oxidation, carburization and hot corrosion during prolonged exposure in temperatures up to 1 300°C. These properties make this alloy a good candidate for high-temperature applications such as gas-turbine combustion chambers, advanced energy conversion systems, diesel engine components, high-temperature shields, and others.[1,2)]

The manufacturing process of commercial ODS alloys usually involves high energy milling of elementary or pre-alloyed metal powders with stable oxides like Y_2O_3 (yttrium oxide). Mechanically alloyed powders are placed in vacuum-sealed cans and consolidated by hot extrusion or hot isostatic pressing at temperatures of about 1 000°C, followed by conventional hot and cold working processes.[3)] A suitable microstructure for high-temperature applications is obtained by subsequent annealing at high temperatures alloys the directional recrystallization is performed under the influence of a high temperature gradient (zone annealing) to promote the formation of elongated grains with a high grain aspect ratio (GAR).[4–7)] This coarse-elongated microstructure is much more creep-resistant than alloys with an equiaxed grain structure.[8)] After zone annealing, MA 956 alloy shows a microstructure consisting of coarse columnar grains parallel to the longitudinal direction (oligocrystalline material). Oligocrystals are polycrystalline aggregates, which consist of a few large grains.[9)] A strong texture resulting from secondary recrystallization process is also present in this alloy.

This peculiar microstructure is found in many cold-workable ODS alloys. The combination of a coarse-grained structure, a strong initial texture, and the presence of fine particles make this alloy a very interesting material for recrystallization studies.

Plastic deformation in coarse-grained materials leads to the development of inhomogeneous microstructures when compared to the relative homogeneity found in fine-grained ones. Individual grains behave quite different during deformation of coarse-grained materials, leading to a very inhomogeneous microstructure. Furthermore, coarse-grained

formation heterogeneities like deformation and shear bands.[10,11] These deformation heterogeneities play an important role during further recrystallization because of the presence of large curvatures associated to these deformation-induced boundaries.

In the present paper we have investigated the microstructural changes and the texture evolution of MA 956 alloy samples deformed by cold swaging. The microstructure of this alloy was characterized by light optical microscopy (LOM), transmission electron microscopy (TEM) and orientation imaging microscopy (OIM) in the as-received and cold-worked conditions. Texture evolution during cold swaging was studied by the X-ray diffraction (XRD) technique. The microtexture of a few selected samples in the deformed state was also investigated using the electron backscattering diffraction (EBSD) technique. The main results of this characterization will be presented and discussed.

2. Experimental Procedure

The results of chemical analyses of the alloy investigated in the present work are given in **Table 1**. The starting material was supplied in bars of 30 mm diameter in the zone-annealed condition. The material was deformed at room temperature in a four-die rotary swaging machine to reductions of 20, 47, 61 and 72% (in area), in multiple passes without intermediary annealing. Samples for metallographic examination were cut from the transverse orientation relative to bar axis. They were ground and polished using conventional techniques. Chemical etching of the polished sections was performed using a V2A-Beize reagent.[12] A chemical method has been chosen for the bulk extraction of the precipitates in MA 956 alloy. The metallic matrix was dissolved in a Berzelius-type solution[13] at 50°C. The solution was filtered through a weighted filter of PTFE. The extraction residue was cleaned in a 0.25 molar hydrochloric acid wash. The structural analysis of the residue was performed by X-ray diffraction using a Cu-Kα1 radiation (λ=0.15405 nm). Microhardness testing was performed in the transversal section of polished samples. The Vickers hardness number (VHN) was determined with a 300-g load. Texture measurements in the deformed samples were carried out by the X-ray diffraction technique using a texture goniometer with Mo Kα1 (λ=0.07093 nm). The microstructure of as-received and cold swaged samples was observed using light optical microscopy (LOM), and orientation imaging microscopy (OIM). Transmission electron microscopy (TEM) investigation in the as-received samples was performed in a Philips CM 120 operating at 120 kV. Thin foils for TEM were electrolytically thinned using a 15% perchloric acid ($HClO_4$)–ethanol solution at 30 V and cooled to 5°C. Orientation imaging microscopy (OIM) results and microtexture investigation were performed by means of automatic indexing of Kikuchi patterns after suitable image processing in a TSL 3.5 system interfaced to Philips XL-30 SEM operating at 30 kV with a W-filament. EBSD sampling points were acquired automatically at steps ranging from 0.5 to 1 μm (step size).

Table 1. Chemical composition (wt%) of the MA 956 alloy used in the present investigation.*

Fe	Cr	Al	Ti	C	S	P	Y
Bal.	19.4	3.8	0.39	0.013	0.0042	0.015	0.42

* Results obtained by X-ray fluorescence technique.

3. Results and Discussion

3.1. Starting Material

The microstructure of the as-received bar is shown in **Fig. 1**. The mean grain size in the transverse section (Fig. 1(a)) determined by the linear intercept method was about 4 mm. Grain boundaries display a serrated morphology as a result of particle-boundary interaction during the manufacturing process. Coarse columnar grains with GAR as high as ≈30 : 1 can be observed in the longitudinal section of Fig. 1(b). It is noticeable the presence of a low fraction of coarse pores (<2% in volume) mostly at grain boundaries. This material is processed by a powder metallurgy route; therefore, these pores likely result from the manufacturing process of this alloy.

Figure 2 shows the (111) pole figure obtained from EBSD mappings based on 70 grains. The alloy presents a predominant ⟨111⟩ texture parallel to the longitudinal direction of the bar. This texture results from secondary recrystallization promoted by zone annealing.

TEM investigation of as-received samples showed a mean particle size of 21 nm. The typical particle interspacing in a plane was found to be close to 53 nm. **Figure 3**(a) shows a TEM micrograph depicting a large population of particles. Two main size classes of particles were observed: smaller particles with sizes ranging from 5 to 100 nm, and coarser particles with sizes ranging up to 500 nm. The size distribution of the smaller particles is shown in Fig. 3(b). The spherical morphology was predominant; however, some cuboidal particles were also observed. The majority of the coarser particles were identified as being $AlYO_3$

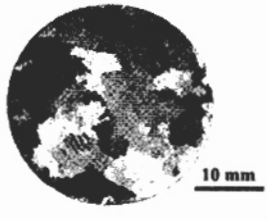

(a)

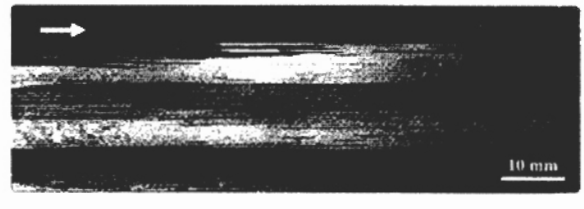

(b)

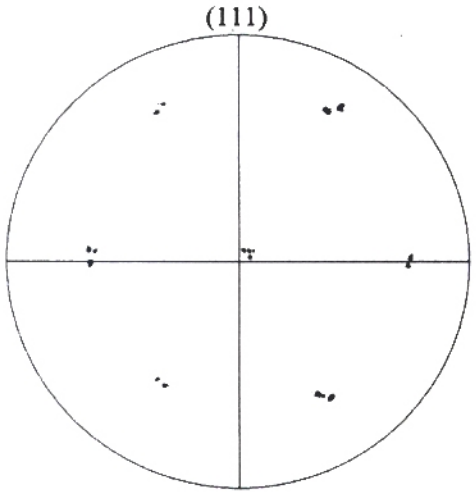

Fig. 2. EBSD (111)-pole figure showing the texture of MA 956 alloy in the as-received condition.

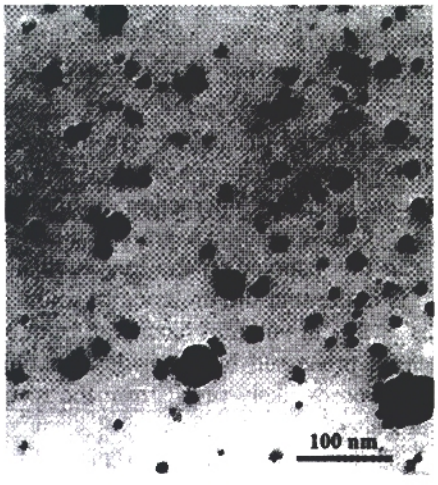

(a)

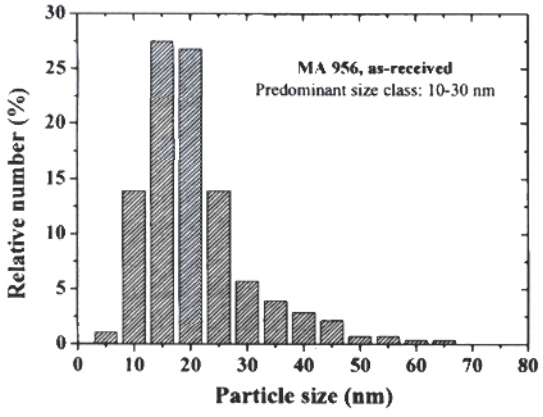

(b)

Fig. 3. Microstructure of MA 956 alloy in the as-received condition: a) TEM micrograph showing particle distribution (transverse section, bright field); b) Size distribution of smaller particles.

(YAP) by EDX analyses in TEM. The structural analysis of

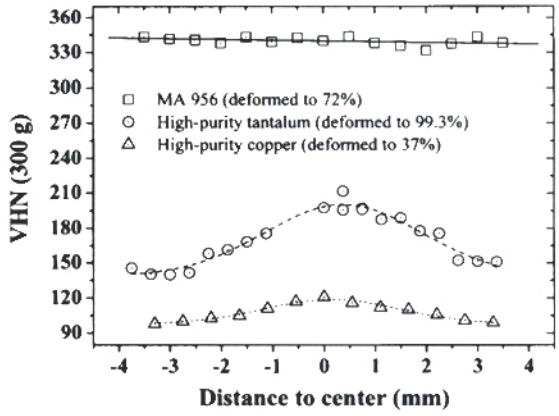

Fig. 4. Microhardness distribution after cold swaging for MA 956 alloy, high-purity tantalum,[19] and high-purity copper.[20]

compounds are considered stable crystalline phases in the Y_2O_3–Al_2O_3 system.[14] These evidences suggest that former Y_2O_3 particles react with aluminum in solid solution during the manufacturing process of the alloy. Similar results were reported in previous works.[15–17] Further details concerning the microstructural characterization of the MA 956 alloy are reported elsewhere.[18]

3.2. Hardness Measurements and the Work Hardening Behavior

Hardness varies from surface to center in many cold-swaged materials. In earlier investigations[19,20] the hardness of copper and tantalum bars deformed by cold swaging, both of high-purity, showed profiles where the center was found to be harder than the surface, as clearly depicted in **Fig. 4**. Figure 4 shows the hardness distributions for MA 956 alloy, high-purity tantalum, and high-purity copper. In the present investigation, hardness measurements showed that work hardening in MA 956 alloy was much more uniform. The hardness values do not change significantly along the diameter of the swaged bars and the relative standard deviation (RSD) values were about 2%. This uniformity is absent in tantalum and copper bars. These results suggest that the stored energy of cold work in MA 956 appears to be homogeneously distributed in a coarser scale. In a finer scale, the dislocation structures found in materials containing a fine dispersion of particles tend to be more homogeneous than in materials without particles.[21] Finer particles sizes and spacings may also retard cell development during deformation.[21,22]

The work hardening behavior of MA 956 alloy during cold swaging is shown in **Fig. 5**. For purposes of comparison, the work hardening curves of other two ferritic materials, a AISI 430 stainless steel[23] and high-purity iron,[24] are shown. It is worthwhile mentioning that the two latter ferritic materials were deformed by cold rolling; however, remarkable differences in terms of hardening are not expected from one deformation mode to another. In a general manner, the materials displayed similar work-hardening behaviors. With increasing strain, hardness increases, tending towards saturation. This behavior is expected to occur in

the hardness values and in the work hardening rate can be attributed to both solid solution and second phase particle strengthening effects. Solid solution strengthening is the major responsible for the differences observed between the high-purity iron and the AISI 430 steel. Since the chemical compositions of MA 956 alloy and AISI 430 steel are roughly comparable, the noticeable hardness differences between these two materials can be attributed to the presence of incoherent second phase particles.[25]

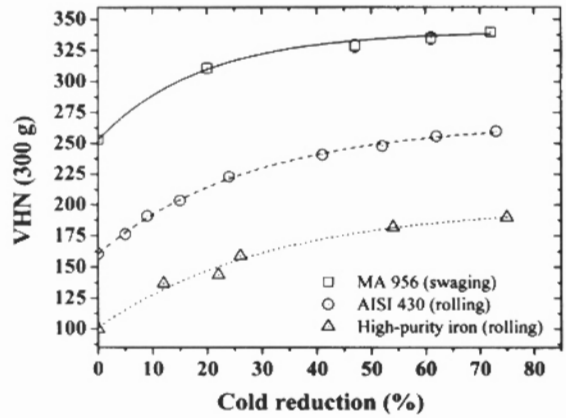

Fig. 5. Work hardening curves for MA 956 alloy, AISI 430 stainless steel,[23] and high-purity iron.[24]

3.3. Microstructure of Deformed Specimens

The microstructural evolution of MA 956 during cold swaging can be seen in **Fig. 6**. These macrographs show the extent of banding with increasing strains. The sample deformed to 72% is fully banded. A closer inspection of the microstructure of the transverse sections of deformed specimens is shown in **Fig. 7**. Banded structures are found in all places in the deformed samples. Deformation bands were observed in most of the grains. The occurrence of deformation banding can be related to grain size and orientation effects.[26] One can see how individual grains behave quite differently during deformation. In Fig. 7 it is possible recognizing grains where banding varies in morphology and spacing. As a rule, these bands lie parallel and are found arranged in colonies. **Figure 8** shows the curly grain structure found in the central regions of samples deformed with reductions above 60%. The curly grain structure is commonly found in transverse sections of bcc metals heavily deformed either by rotary swaging or by wire drawing processes.[27]

The microstructure of deformed specimens slightly varies from the grain boundary into the interior of the grains, especially in coarse-grained materials. This phenomenon was observed to occur in many cases, as depicted in **Fig. 9**. The band spacing of the upper grain (grain A) diminishes when grain boundary approaches (marked by a

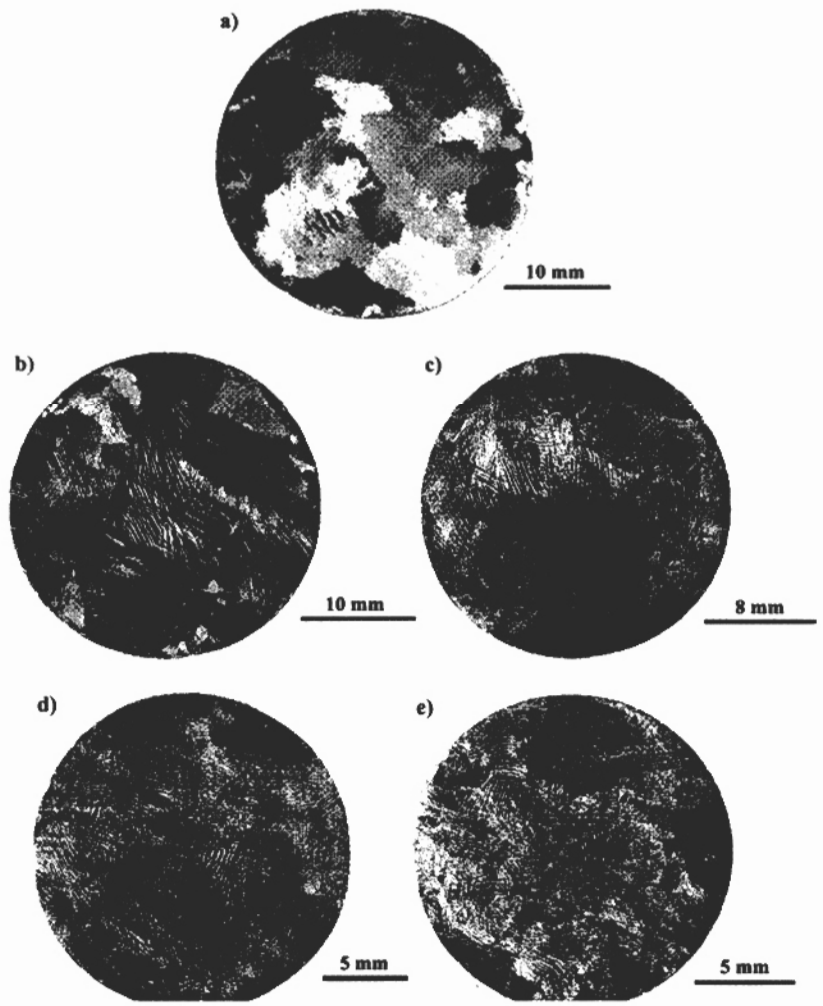

(a)

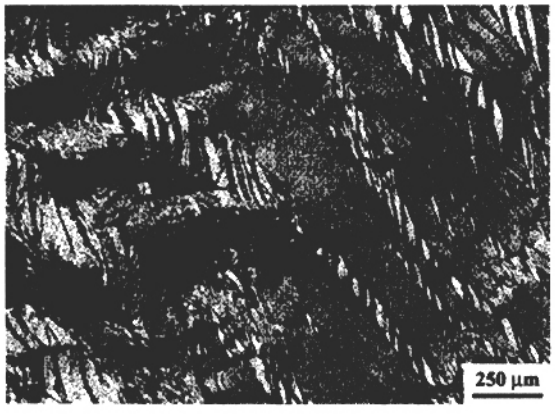

(b)

Fig. 7. Transverse sections of deformed samples showing banded regions: a) 47% reduction; b) 72% reduction (LOM). Note the differences in terms of grain subdivision in adjacent grains.

Fig. 8. Transverse section of sample deformed to 72% reduction showing the curly grain structure (LOM).

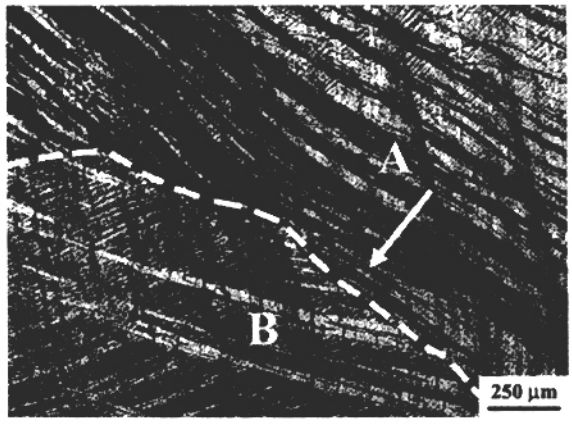

Fig. 9. Detail of grain boundary region in a sample deformed to 47% reduction (LOM).

dashed line). Grain boundary (GB) regions are harder (higher stored energy) than grain interiors for two reasons, as pointed out by Hirth.[28] Firstly, the elastic stresses are greater there making flow harder. Latter, the dislocation structure evolved at GB regions tend to be more complex increasing the stresses for further dislocation slip. The compatibility of deformation between adjacent grains leads to the activation of at least five independent slip systems (Taylor model), resulting in a more intensive dislocation interaction at grain boundary regions. In addition to the higher stored energy found at GB regions, large curvatures are also present making these regions as potential sites for recrystallization upon static annealing. Further EBSD studies are in progress to explain this unusual structure at grain boundaries.

3.4. Deformation Texture

The texture evolution during cold swaging of MA 956 alloy was studied by the X-ray diffraction technique (XRD). The (110) and (200) pole figures were recorded in a texture goniometer. Results show that the initial ⟨111⟩ texture evolves towards a sharp ⟨110⟩-fiber texture during cold swaging, *i.e.*, the ⟨110⟩ directions tend to align in a direction parallel to the bar axis. **Figure 10** clearly shows the progressive concentration of iso-density lines at 60° and creases from TR=9.1 (sample deformed to 20% reduction) to TR=15.4 (sample deformed to 72% reduction). The symmetry presented by (110) and (200) pole figures for the sample deformed to 72% reduction allowed the calculation of the respective orientation distribution function (ODF), showed in **Fig 11**. The ⟨110⟩-fiber texture is evidenced in the φ_2 sections of 0° and 90°, for ϕ=45°. The maximum orientation density (TR) was 17.4. Curling of grains is necessary to accommodate the flow of individual grains in bcc metals.[29] This peculiar structure has to do with the development of a pronounced ⟨110⟩ texture in bcc metals deformed by wire drawing or cold swaging. There are only a few works in the literature concerning texture evolution during cold working in ODS materials. Réglé[30] reported similar results for MA 956 samples deformed by cold swaging to reductions of 20 and 60%.

3.5. EBSD Mappings

The characterization of deformed samples using EBSD revealed many interesting aspects concerning the microstructural evolution of this alloy during deformation by cold swaging. Orientation maps from EBSD data corresponding to samples deformed to 20 and 47% are presented respectively in **Figs. 12** and **13**. The OIM maps of Figs.

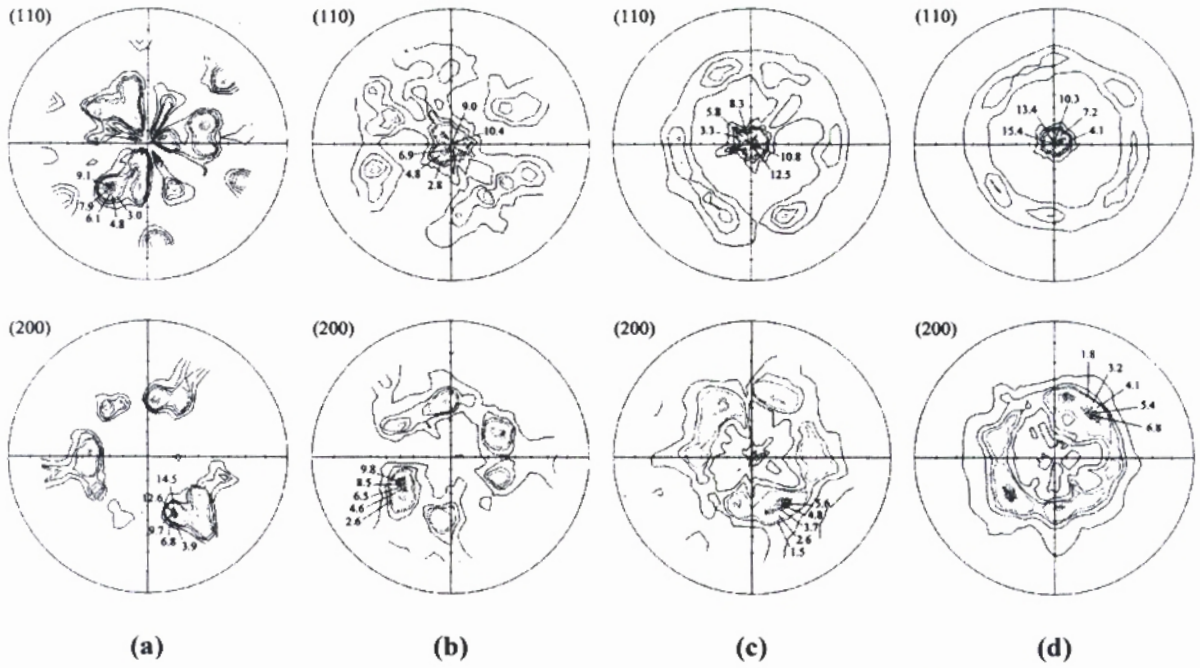

Fig. 10. Texture evolution during cold swaging of MA 956 alloy. (110) and (200) pole figures for samples deformed to: a) 20% reduction; b) 47% reduction; c) 61% reduction; and d) 72% reduction.

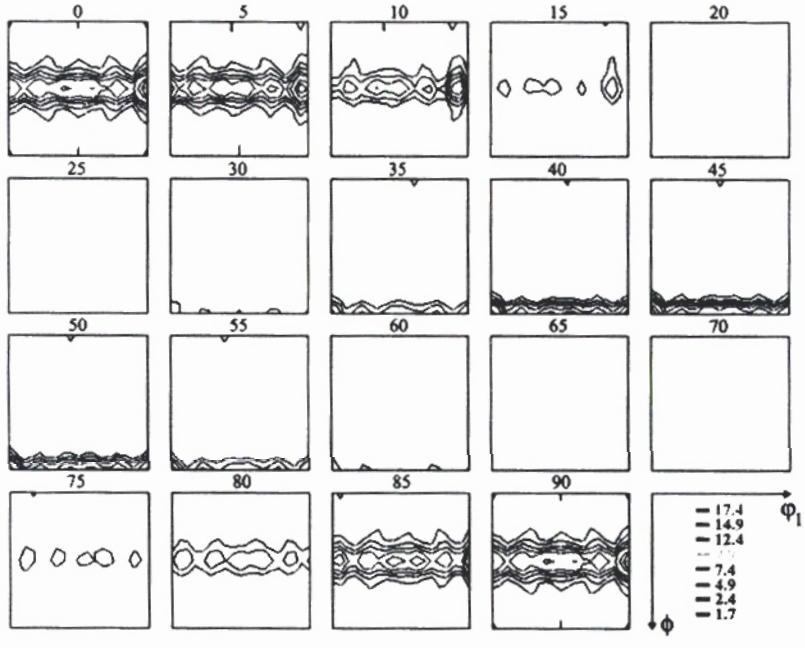

Fig. 11. Orientation distribution function (ODF) calculated for the sample deformed to 72%.

by deformation bands. Low-energy coherent Σ-3 boundaries, a characteristic feature of deformation twins, were not found throughout the banded structure. The image quality (IQ) map of Fig. 12(b) shows that the majority of the mapped points could be properly indexed. When dislocation density increases, Kikuchi patterns become more diffuse and cannot be properly indexed. In the IQ map shown in Fig. 13(b) (47% reduction), it may be observed a significant increase in the amount of crystalline defects (darker regions).

The curvature associated to deformation bands (DBs) tion banding varies from 10 to 19°, approximately. The regions between these bands display low curvatures, in average below 2°. A second mapping was performed in a more deformed specimen (47% reduction). The misorientation profile shown in Fig. 13(c) (referring to the line test 2 shown in Fig. 13(a)) clearly indicates larger curvatures. Misorientation across DBs rises to about 30°. This curvature has a high-angle character. EBSD mapping could not be performed in samples deformed to 61 and 72% reductions because of the poor quality of acquired Kikuchi patterns.

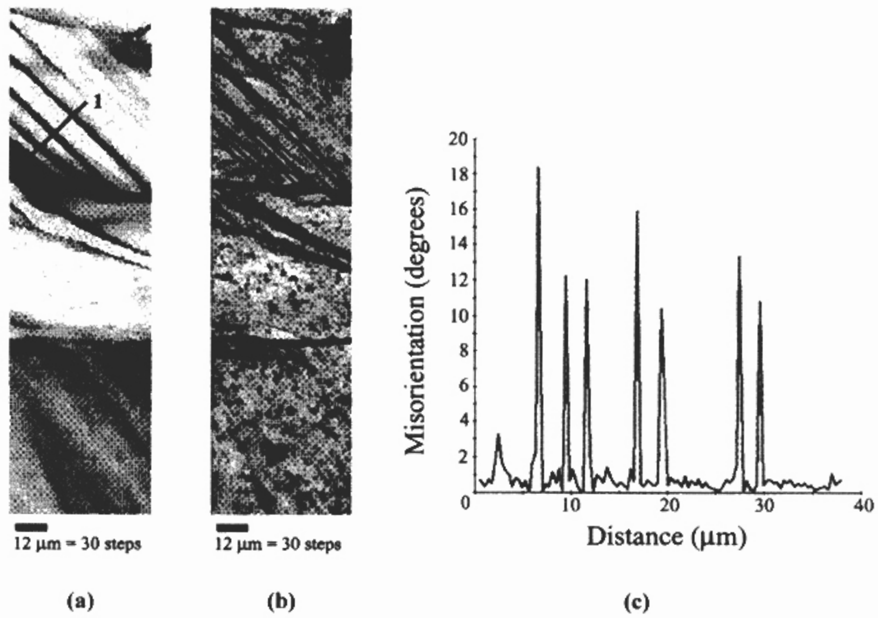

Fig. 12. EBSD mapping of a sample deformed to 20% reduction: a) OIM showing details of its microstructure; b) IQ map; c) misorientation profile corresponding to line test 1 (transversal section).

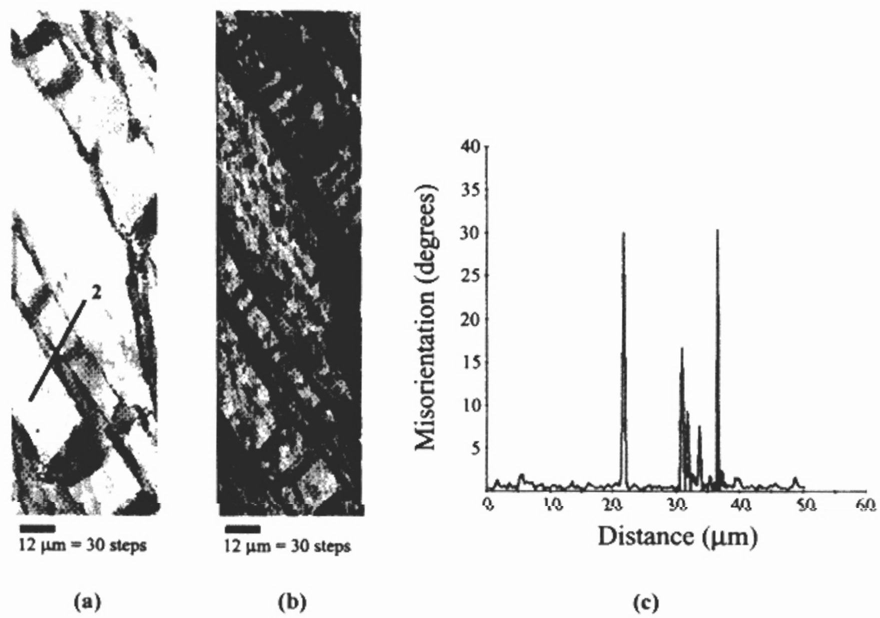

Fig. 13. EBSD mapping of a sample deformed to 47% reduction: a) OIM showing details of its microstructure; b) IQ map; c) misorientation profile corresponding to line test 2 (transversal section).

coarse-grained materials.[31)] At this point, it is opportune to emphasize that the total area of boundaries provided by deformation bands is much larger than the whole grain boundary area available in coarse-grained materials.[32)] This aspect will be discussed in Part II.

4. Conclusions

The following main conclusions can be drawn with regard to the microstructural characterization of as-received and cold swaged samples of MA 956 alloy:

(1) MA 956 superalloy in the as-received condition displays ... longitudinal direction of the bar.

(2) The former Y_2O_3 particles react during the manufacturing process of the alloy, giving rise to a mixture of yttrium-aluminates. X-ray diffraction analysis of the extracted particles showed the predominance of $AlYO_3$ (YAP) and $Y_3Al_5O_{12}$ (YAG) compounds.

(3) Cold swaging of oligocrystalline MA 956 alloy leads to the development of an inhomogeneous microstructure. Deformation banding was observed to occur in all grains. Band morphology and spacing varied from one grain to another. Curvatures associated to DBs were determined by EBSD measurements reaching values of about

sociated to these planar DB boundaries is much larger than the one corresponding to grain boundaries.

(4) With increasing strain, grains tend to display the so-called curly structure and develop a sharp ⟨110⟩-fiber texture during cold swaging. This deformation texture was strengthened with the increase of the applied strain.

Acknowledgements

The authors are grateful to FAPESP (Sao Paulo, Brazil) for supporting this work (Grant No. 99/10793-8 and 99/06458-0). M. F. Hupalo acknowledges FAPESP for his Post-Doctoral scholarship under Contract No. 03/04046-3. Thanks are also due to Dr. W. K. Reick (Ruhr-Universituät Bochum, Germany) for supplying the MA 956 alloy bars. H. R. Z. Sandim is CNPq fellow under Contract No. 300.158/02-5.

REFERENCES

1) INCOLOY alloy MA 956, Special Metals Corporation, Huntington, USA, (2000).
2) H. D. Hedrich: Proc. Conf. New Materials by Mechanical Alloying Techniques, ed. by E. Arzt and L. Schultz, Informationsgesellschaft Verlag, Erlangen, (1988), 217.
3) H. K. D. H. Bhadeshia: *Mater. Sci. Technol.*, **16** (2000), 1404.
4) C. P. Jongenburger and R. F. Singer: Proc. Conf. New Materials by Mechanical Alloying Techniques, ed. by E. Arzt and L. Schultz, Informationsgesellschaft Verlag, Erlangen, (1988), 157.
5) M. M. Baloch and H. K. D. H. Bhadeshia: *Mater. Sci. Technol.*, **6** (1990), 1236.
6) M. Mujahid and J. W. Martin: *Mater. Sci. Technol.*, **10** (1994), 703.
7) M. A. Miodownik, J. W. Martin and E. A. Little: *Mater. Sci. Technol.*, **10** (1994), 102.
8) E. Arzt: *Res. Mech.*, **31** (1990), 399.
9) D. Raabe: *Steel Res.*, **66** (1995), 222.
10) N. Hansen: *Scr. Metall. Mater.*, **27** (1992), 1447.
11) F. J. Humphreys and M. Hatherly: Recrystallization and Related Annealing Phenomena, Pergamon, Oxford, (1995), 21.
12) G. Petzow: Metallographic Etching, ASM International, Metals Park, Ohio, (1978), 131.
13) K. E. Burke: *Metallography*, **8** (1975), 473.
14) X. Guo and K. Sakurai: *J. Mater. Sci. Lett.*, **19** (2000), 451.
15) A. Alamo, H. Réglé, G. Pons and J. L. Bechade: *Mater. Sci. Forum*, **88–90** (1992), 183.
16) H. Cama and T. Hughes: Proc. of Materials for Advanced Power Engineering, Part II, Kluwer Academic Publishers Group, Dordrecht, (1994), 1497.
17) B. Dubiel, W. Osuch, M. Wróbel, P. J. Ennis and A. Czyrska-Filemonowicz: *J. Mater. Process. Technol.*, **53** (1995), 121.
18) M. F. Hupalo, M. Terada, A. M. Kliauga and A. F. Padilha: *Mater.wiss. Werkst.tech.*, **34** (2003), 505.
19) J. Schrank: *Mater. Sci. Technol.*, **1** (1985), 544.
20) M. F. Hupalo and H. R. Z. Sandim: *Mater. Sci. Eng. A*, **A318** (2001) 216.
21) F. J. Humphreys and M. Hatherly: Recrystallization and Related Annealing Phenomena, Pergamon, Oxford, (1995), 243.
22) E. Hornbogen and U. Köster: Recrystallization of Metallic Materials, ed. by F. Haessner, Dr. Rieder Verlag GmbH, Stuttgart, (1978), 159.
23) A. F. Filho, F. C. Pimenta Jr, A. F. Padilha, N. B. de Lima and M. F. Hupalo: Proc. of 40th Rolling Seminar: Process, Rolled and Coated Products, ABM, São Paulo, Brazil, (2003), 262.
24) X. J. Hao, Z. G. Liu, K. Masuyama, T. Rikimaru, M. Umemoto, K. Tsuchiya and S. M. Hao: *Mater. Sci. Technol.*, **17** (2001), 1347.
25) M. F. Ashby: Strengthening Methods in Crystals, ed. by A. Kelly and R. B. Nicholson, Applied Science Publishers, London, (1971), 137.
26) C. S. Lee, B. J. Duggan and R. E. Smallman: *Acta Metall. Mater.*, **41**, (1993), 2265.
27) A. T. English, G. Y. Chin and B. C. Wonsiewicz: ASM Handbook, Vol. 8, ASM, Materials Park, Ohio, (1973), 211.
28) J. P. Hirth: *Metall. Trans.*, **3** (1972), 3047.
29) W. F. Hosford, Jr.: *Trans. AIME*, **230** (1964), 12.
30) H. Réglé: PhD Thesis, Université de Paris-Sud, UFR Scientifique D'Orsay, Paris, (1994), 196.
31) H. R. Z. Sandim, J. F. C. Lins, A. L. Pinto and A. F. Padilha: *Mater. Sci. Eng. A*, **A350** (2003), 217.
32) D. Kuhlmann-Wilsdorf, S. S. Kulkarni, J. T. Moore and E. A. Starke Jr.: *Metall. Trans. A*, **30A** (1999), 2491.